SCIENTIFIC PAPER

Innovative aberration correction in ultrasound diagnostics with direct phase estimation for enhanced image quality

Denis Leonov[1,2] · Nicholas Kulberg[3] · Tatyana Yakovleva[3] · Polina Solovyova[2] · José Francisco Silva Costa-Júnior[4] · Manob Jyoti Saikia[5]

Abstract

The paper addresses a crucial challenge in medical radiology and introduces a novel general approach, which utilises applied mathematics and information technology techniques, for aberration correction in ultrasound diagnostics. Ultrasound imaging of inhomogeneous media inherently suffers from variations in ultrasonic speed between tissue. The characteristics of aberrations are unique to each patient due to tissue morphology. This study proposes a new phase aberration correction method based on the Fourier transform and leveraging of the synthetic aperture mode. The proposed method enables correction after the emission and reception of ultrasonic wave, allowing for the estimation of aberration profiles for different parts of the sonogram. To demonstrate the method's performance, this study included the conducting of experiments using a commercially available quality control phantom, an *ex-vivo* temporal human bone, and specially designed distortion layers. At a frequency of 2 MHz, the experiments demonstrated an increase of two-and-three-quarters in echo signal intensity and a decrease of nearly two-fold in the width of the angular distribution compared to the pre-correction state. However, it is important to note that the implementation of the method has a limitation, as it requires an aperture synthesis mode and access to raw RF data, which restricts use in common scanners. To ensure the reproducibility of the results, this paper provides public access to an in-house C++ code for aberration correction following the proposed method, as well as the dataset used in this study.

Keywords Focused ultrasound · Phase correction · Phantom · Synthetic aperture · Beam formation · Medical imaging

✉ Denis Leonov
leonovd.v@ya.ru

José Francisco Silva Costa-Júnior
francisco@sbeb.org.br

Manob Jyoti Saikia
manob.saikia@unf.edu

1 Moscow Center for Diagnostics and Telemedicine, Moscow, Russia

2 National Research University "Moscow Power Engineering Institute", Moscow, Russia

3 Federal Research Centre "Computer Science and Control" of the Russian Academy of Sciences, Moscow, Russia

4 Brazilian Air Force Academy, Pirassununga, São Paulo, Brazil

5 Department of Electrical Engineering, University of North Florida, Jacksonville, FL 32224, USA

Introduction

It has been demonstrated that the unavoidable presence of distortion in diagnostic images has represented a significant bottleneck concerning increasing the quality of diagnostic capability in medical radiology devices. These distortions, are caused by aberrations in the signal being visualised. This paper considers this problem specifically in the context of ultrasound diagnostics, which widely regarded as the most commonly used modality in medical radiology.

The skull's thickness and density vary from patient to patient. The presence of these a priori unknown structural inhomogeneities leads to inevitable distortions of the beam and a poor diagnostic ultrasound image. Thus, as shown in ref. [1], ultrasound echo-signal aberrations were revealed based on the evaluation of the beam's width and comparing this parameter with its theoretically calculated value. However, revealing the presence of aberrations alone does not improve focusing quality. After being revealed, aberrations should also be corrected. Therefore, this paper presents

a general approach to correcting aberrations and uses the previously reported detection approach [1] to estimate the degree of correction. This novel approach is based on the Fourier transform technique for extraction of phase information for aberration correction [2–4]. Phase aberrations are distortions of the wavefront that occur due to differences in wave propagation speeds in inhomogeneous media. The presence of phase aberrations leads to poor spatial and contrast resolutions [5]. At a higher frequency, phase aberrations and ultrasound attenuation become more prominent. Therefore, lower frequencies are preferable, although lower frequencies result in widening of the focal spot and decreasing of the resolution.

To achieve better image quality, phase aberration correction methods are necessary. Several correction methods were proposed, based on time-shift [6, 7] and a wavefront reversal technique [8]. However, these methods require either the presence of bright point reflectors or a point source in the focal area [9]. This can be achieved by introducing a miniature source such as contrast agent bubbles through blood vessels [10, 11] or cavitation bubbles [12]. As introducing a source within the human body can be challenging and sometimes impossible, several additional aberration correction techniques were proposed.

Philips et al. [13] and Vignon et al. [14] placed a second transducer on the other side of the body part; thus, they were able to correct the region of interest (ROI) lying on the axis between both probes. Later, Lindsey and Smith [15] reproduced a method for obtaining 3D Doppler ultrasound images of blood flow in the circle of Willis. One of the implementation variants of this method [16] was used in our study as a reference method. However, placing probes on both sides of the body part does not allow for optimal focus on every existing point inside the frame, which makes the approach unsuitable for heterogeneous media. These methods rely on the unrealistic assumption that the phase delays induced by aberrations do not change over the entire field of view, but they can still serve as a sound approximation regardless of the limitations.

Other noninvasive methods have been proposed in the literature. These methods include measuring the resonant frequency for specific skull thickness [2], determining the optimal transmission frequency [3, 4], and 3D printing an acoustic lens to compensate for aberrations [17, 18]. Researchers then recognised the potential of computed tomography (CT) and magnetic resonance imaging (MRI) in determining the acoustic properties of the skull, leading to proposals for a new set of noninvasive methods [2, 19, 20]. In ref. [19], CT images were used to determine the density, thickness, and absorption coefficient of the human skull. This information was incorporated into a 3D finite difference numerical simulation along with a time reversal method to correct for phase and amplitude aberrations induced by

the skull. In essence, the computer simulation eliminated the need for an ultrasonic source at the focal point of the transducer.. Instead, a virtual point-like source was used, emitting a pulse that was numerically propagated through the skull to the transducer via the finite difference method. Subsequently, the recorded signals were reversed in time and reemitted. In summary, these advancements in computer simulation offer promising alternatives to traditional methods, bypassing the need for physical ultrasonic sources and enabling accurate corrections for aberrations in noninvasive ultrasound imaging.

The current study investigates the drawbacks of the described techniques and proposes a new method to correct phase aberrations. The initial step of the new method was the previously reported approach [1] to detect the presence of aberrations. These aberrations were then corrected by calculating the phase spectrum and applying appropriate delays during beamforming. To detect the presence of aberrations, our approach created virtual point sources, thereby enabling correction regardless of the presence of the real sources or bright reflectors. These virtual point sources were employed to assess the quality of focus. When the focusing was fine, meaning that aberrations were absent, the virtual point sources appeared as sharp dots on a sonogram. However, when aberrations were present, the virtual point sources became blurry, characterised by a wider and less bright appearance. If the sources appeared blurry, aberration correction was applied, resulting in a new ultrasound image with corrected phase. By implementing this method, we aimed to overcome the drawbacks of previous techniques and improve the accuracy of phase aberration correction in ultrasound imaging.

A recent approach, proposed by Lambert et al. [21], also utilised virtual sources for aberration correction. They introduced a distortion matrix approach, which can overcome the limitations of dual probe correction [14]. This current paper can thus be seen as a further development of the method presented by Lambert et al. For the operation of this method, a special diagnostic scanning scheme was used in synthetic aperture mode. Using this scheme, the Fourier transform of the aperture function was created in the focal plane. The aperture function represents the intensity of the signal passing through the aperture, which makes it possible to estimate aberration profiles separately for different parts of the sonogram. The principle of aperture synthesis, as implemented in this study, means that pulses are emitted sequentially by each element but received by all probe elements simultaneously. This allows for the setting of any required focal lengths by changing the corresponding delays of the preliminarily stored unfocused signals. The performance of the aberration correction method proposed in this study was evaluated by comparing the intensity of the echo signal and

the width of the angular distribution (which represents the dependency of the echo signal intensity on the angle of inclination) obtained using the proposed method with those obtained using the reference method [16]. Additionally, experimental results at 2 MHz carrier frequency using an ATS phantom, an *ex-vivo* temporal bone, and specially designed distortion layers were presented.

Materials and methods

Principles of synthetic-aperture imaging

The synthetic aperture method, unlike conventional beam-forming, where only one or a few focal depths are achieved, can provide multiple focal depths and finer resolution [22]. This method implements a scanning sequence where a single element emits a signal and multiple elements simultaneously receive echoes of this signal, then the sequence repeats for the next element and so on until every element has completed emitting a signal. This generates an unfocused dataset, which can be used to mathematically focus on each spatial point by performing coherent summation. Moreover, this method offers the flexibility to focus during the post-processing stage, which is essential for aberration correction techniques. In our method of aberration correction, we used a variation of synthetic aperture imaging, which treats focal positions as virtual point sources, as first proposed in ref. [23]. This method is effective even for purely virtual sources, regardless of the existence of a real source or a strong reflector, thus, eliminating the need for reflectors such as a wire inside a phantom.

Proposed method for aberration correction

The proposed method for aberration correction is schematically illustrated in Fig. 1. A scanning process is conducted in synthetic aperture mode [24], and, subsequently, a region of interest (ROI) is selected. This process generates a set of unfocused data, which is then transferred to a personal computer. Data processing on a computer has two steps. An algorithm, presented in the section "Automatic detection of the presence of aberrations in sonograms", performs the first step of the processing. This algorithm detects aberrations in ultrasound images without human intervention. A new algorithm, presented in the section "Estimation of the phase delays compensating for aberrations", performs the second step of processing. The aim of this algorithm is to estimate phase delays, which are then used to compensate for aberrations. Finally, a high-quality image of the ROI is constructed, as shown in Fig. 1.

Automatic detection of the presence of aberrations in sonograms

The proposed method of aberration correction utilises a specialised diagnostic scanning scheme to create virtual point sources, allowing for the estimation of aberrations regardless of the presence of real point reflectors. The scanning unit creates these sources by focusing on a single spatial point during transmission while scanning the entire frame during reception [1]. To detect the presence of aberrations, the angle of the transmitted beam should be aligned and fixed in such a way that it passes through the centre of the selected ROI. The resulting frame exhibits a single point spread function in the focal area. This point spread function is sharper in the absence of aberrations and blurs in their presence.

In practice, to reduce the impact of speckle noise, data were accumulated from multiple virtual point spread functions located along the beam. The resulting image appeared as the brightest possible line along the beam if there were no aberrations. This corresponded to the angle chosen for the transmitter beam. As shown in the comparison of the branches in the "Is there a distorting layer?" section in Fig. 1, the presence of aberrations widened the line and blurred the brightest area. This widening of the line and blurring of the brightest area occurred because the presence of aberrations widens both the transmitter and receiver beams. This widening was automatically compared with the theoretical width of the point spread function in the absence of aberrations. If the estimated width of the virtual point spread function exceeded the linked theoretical width threshold, then the correction procedure was conducted. A detailed explanation of the aberration detection approach is provided in [1].

Estimation of the phase delays compensating for aberrations

The essence of the proposed aberration correction method was that the response function of the virtual point source contains the necessary information to restore the aberration profile. To extract this profile, a one-dimensional Fourier transform was applied to the horizontal line of the B-scan, which intersects the virtual point source. The result of the Fourier transform provided the amplitude and phase spatial distributions, with the phase spatial distribution indicating the required aberration profile. To denoise the resulting phase estimation, the operation of calculating the phase spatial distribution was applied to several virtual points positioned in the same isoplanatic patch, and the results were accumulated.

Mathematically, the proposed aberration correction procedure was composed of several steps. First, a matrix of complex numbers $W_{m,n}$ was obtained from the beamformer output, where m was the number of beams and n was the
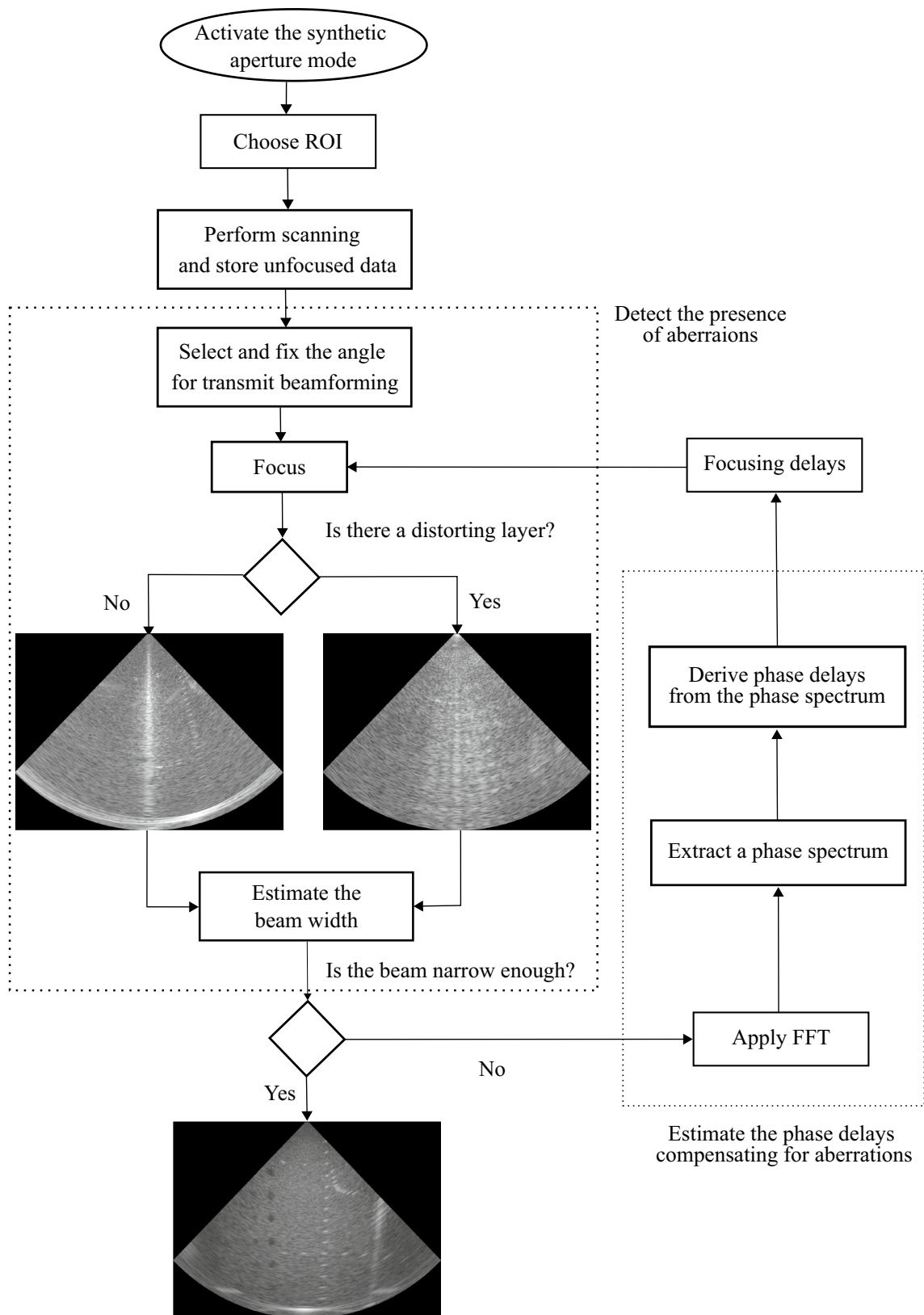
Fig. 1 A flow chart summarising the proposed process of aberration correction

number of samples corresponding to the depths. This matrix was obtained using the special diagnostic scanning scheme creating multiple focuses. The focuses for these measurements must be far apart enough to ensure a degree of statistical independence but constrained in space by the isoplanatic requirement [25]. Then, the phase distortion for each element of the transducer aperture was estimated following the procedure outline next.

The calculation of the Fourier transform $\mathcal{F}$ of the matrix of complex numbers $W_{m,n}$ resulted in:

$$P = \mathcal{F}(W) \tag{1}$$

Then the matrix of phase derivatives $I_{m-1,n}$ were calculated for the transformed matrix:

$$I_{k-1,i} = arg\left(P_{k,i} \cdot \overline{P_{k-1,i}}\right) \tag{2}$$

where arg is the argument operator of a complex number; $P_{k,i}$ is the element of the complex matrix P; $\overline{P_{k-1,i}}$ is the element with the number $k-1, i$ of matrix P obtained as a result of complex conjugation; k is the beam number, $k = 1 \ldots m-1$; and i is the sample number, $i = 1 \ldots n$.

Next, the rows of the phase derivatives matrix were obtained and the vector E_{m-1} was determined:

$$E_k = \frac{1}{n}\sum_{i=1}^{n} I_{k,i} \tag{3}$$

where E_k is the k-th element of the accumulation vector of phase derivatives. This accumulation denoised the estimates.

The phases vector Z with the dimension of $m-1$ was calculated by adding the sum of previous elements to each subsequent element of the accumulation vector of phase derivatives E:

$$Z_k = \sum_{i=1}^{k} E_i \tag{4}$$

where Z_k is the k-th element of the phase vector.

From the resulting vector Z, a new vector of phases G is created by repositioning the elements and discarding those lying outside the spectrum boundaries:

$$\begin{cases} j = 1; \\ for\, i\, from\, \frac{m}{2}\, to\, (m-1)\, if\, \frac{\Theta}{m}\left(i - \frac{m}{2}\right) \le \frac{\Delta}{2}\, do\, \left\{G_j = Z_i\, and\, j = j+1\right\}; \\ for\, i\, from\, 1\, to\, \frac{m}{2}\, if\, \frac{\Theta}{m}\left(\frac{m}{2} - i\right) \le \frac{\Delta}{2}\, do\, \left\{G_j = Z_i\, and\, j = j+1\right\}, \end{cases} \tag{5}$$

where G_j is the element with the number j of the new vector of phases; Δ is the spectrum width; and Θ is the angular value of the scanning sector, which is equal to $\pi/2$ in our experiments.

The discarding criterion, that is, the spectrum width, was calculated using the formula:

$$\Delta = \frac{2\pi\lambda}{w} \tag{6}$$

where w is the aperture width and λ is the wavelength.

Next, a cubic spline interpolation of the obtained phase vector G was performed to obtain a set of correction delays Ψ_{prop} using our proposed method. The number of elements in this delay vector Ψ_{prop} was equal to the number of receiver elements of the ultrasound transducer:

$$\psi_{prop} = interp(G) \tag{7}$$

where $interp$ is the operator for calculating the interpolated values of the vector. This resulting a set of correction delays was used to correct phase distortions in the selected isoplanatic patch.

Thus, the principle of the proposed approach to correcting the aberrations was founded on the notion that the lateral representation of the signal in the focal plane can be expressed as the Fourier transform of the aperture function. The aberrating layer in our model was conceptualised as a complex-valued function that multiplies the signals on the aperture. Our observations indicate that the aberration distortions are primarily caused by phase fluctuations in the aberrator function. Therefore, to correct these distortions, phase correction was applied to the lateral Fourier transform of the signal in the focal plane [26, 27].

Reference method for aberration correction

This method [16] implements the time reversal mirror approach [9], which means it is based on the use of a second (reference) probe attached to the phantom surface opposite the first (multi-element) probe (Fig. 2). The aberration correction procedure was performed prior to obtaining the resulting sonogram. This procedure includes emitting a pulse with the reference probe. A pencil-type ultrasound transducer with a single element with a circular aperture surface of 3 mm² was used as the reference probe; it acted as a nearly point-like source and emitted pulses at a carrier frequency of 2 MHz. As the emitted pulse traversed the ROI, it reached the elements of the multi-element probe. The system measured and stored delays for this emitted signal, and the beamformer used these delays to focus the multi-element probe on the reference probe. If the amplitude of the signal
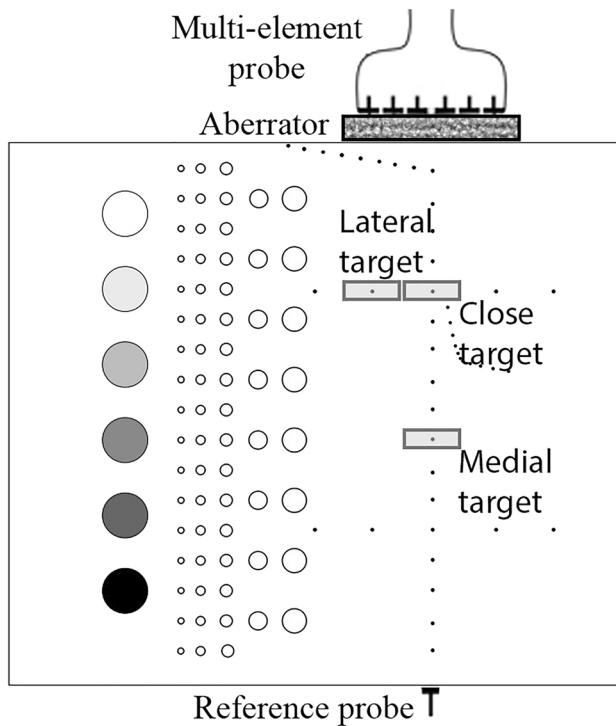
Fig. 2 Positioning of the probes according to the reference aberration correction method in relation to the distortion layer and ultrasound phantom

received by the reference probe was sufficient, the aberration correction procedure was considered complete, and the beamformer employed the obtained delays to scan the entire frame. Note that the conventional time reversal technique [8] does not require delay calculation, and directly reverses the received signals, but does require the placement of a source inside the phantom. This could not be done, therefore, the delays measured for the small probe on the surface were used to scan the area inside the phantom.

Ultrasound system

In this study, a Sonomed-500 research ultrasound scanner (Spectromed, Moscow, Russia) was used to transmit raw data from the synthetic-aperture B-mode path to a personal computer (i5-8400 CPU operating at 2.81 GHz and 16 GB RAM) for further processing. In addition, a 3.0S19 sector probe (Medelcom, Vilnius, Lithuania) with a width of 13 mm, and having 64 elements with a pitch of 290 μm, a − 3 dB bandwidth of 1.6–3.7 MHz, and operating at 2 MHz carrier frequency was employed for scanning.

Phantom and aberrators

Figure 2 illustrates the configuration on targets of a multipurpose phantom (Model 539, ATS Laboratories, USA)

used in the study. The phantom contains nylon strings for spatial resolution evaluation, which makes it suitable for measuring the performance of the proposed aberration correction technique. The speed of sound and attenuation measured at 2 MHz in the phantom were 1450 m/s and 0.5 dB/cm/MHz, respectively.

In each of the conducted experiments, one of three distorting layers was employed. Two of these layers measured $35 \times 26 \times 2$ mm each and were created using LCD 3D printing technology [28]. They were specifically designated aberrator #1 and aberrator #2 in the study and were made from photopolymer Industrial Blend by Funto-Do (the Netherlands). The third layer, referred to as aberrator #3, was an *ex-vivo* temporal human bone model approximately 70×50 mm in size with a thickness of less than 4 mm and a density of 1450 mg/cm^3. The temporal human bone model was obtained from a medical university laboratory, where it underwent cleaning and was frozen for several months. The speed of sound and acoustic attenuation at 2 MHz in the resin were 2400 m/s and 5 dB/cm/MHz, respectively, which is comparable with the outer table of the skull bone [29]. The shapes of the photopolymer aberrators were obtained via the harmonic function:

$$A \cdot sin\left(180° \cdot l/L + \gamma_0\right) \tag{8}$$

where γ_0 was the initial phase equal to 180°, A was the amplitude equal to 500 μm, L was the aperture width of the phased array probe, and l was the distance from the origin. One-and-a-half periods and two-and-a-half periods of the function were able to fit on the surface of the first and second plates, respectively. Thus, both resin aberrators were homogeneous; the only difference between them was their shape. The aberrations introduced by these plates were estimated and compared to those created by the *ex-vivo* temporal bone. Aberrators #1 and #2 yielded root mean square (RMS) values of 39 and 97, respectively. Thus, aberrator #2 was slightly stronger than would be expected in an *invivo* observation, as an RMS in the temporal bone model presented by aberrator #3 was 44 ns and, according to the literature [30], the mean RMS in skull samples has been found to be 60 ns. It is worth noting that the temporal skull bone represented by aberrator #3 had irregular thickness. Its distortion profile changed along the lateral and elevational coordinate, while the distortion profiles of the photopolymer aberrators changed along the lateral coordinate and did not change along the elevational coordinate. Thus, aberrators #1 and #2 were simplified models. Although they posed some of the properties of skull bones, they were not intended to mimic any specific tissue but served as a general model. They allowed us to better predict and verify the aberration profiles estimated in the correction process.

Just before the experiments, aberrators #1 and #2 underwent a 30-min degassing process in the vacuum chamber with the air pressure maintained at less than 2 ppm using a pump (VALUE VE-2100, China). The temporal bone model was rinsed with deionised water and then rehydrated overnight in degassed deionised water inside the vacuum chamber to remove air. The ultrasound sector probe was securely mounted on a tripod to minimise unwanted vibrations and position it accurately. To attach the distorting plates to the ultrasound probe, a custom holder was 3D printed from PLA plastic. To fit the holder snugly on the probe, 3D scans of the probe were performed, and this information was used for 3D printing. The aberrator was attached to the holder under the emitting surface of the probe, using a special fastener on the printed holder.

Experimental procedure

First, the sector probe was placed on the phantom's surface such that the ROI covered the target. The space between the emitting surface of the probe and the phantom was filled with degassed water. The scanning was performed in the synthetic aperture mode, and an array of unfocused data was generated of the size $d \times d \times g$, where d was the number of probe elements and g was the number of samples. This data array obtained for a case without a distortion layer was transferred to a personal computer for further processing and generation of a sonogram.

Then, a distortion layer, that is, the aberrator, was placed in the space between the probe surface and the phantom. For this step, the plastic holder with the previously mentioned specific fastener was put on the probe. The same scanning procedure described in the previous paragraph for the case without aberrations was repeated here for each of the three distortion plates. These acquired data arrays were also transferred to a personal computer. In total, the data acquisition process was repeated five times for each aberrator and the case without a distorting layer. Before each repetition, the probes were relocated away from the phantom and then put back so that their relative positions could vary slightly.

In-house C + + code was run on a personal computer in the Microsoft Visual Studio environment read the data and built the sonograms for each of the arrays of unfocused data. These sonograms were built without performing any aberration correction. Next, for each of the data arrays

obtained with the distortion plates, a correction was performed in each ROI according to the procedure described earlier in the "Proposed method for aberration correction" and "Reference method for aberration correction" sections. For each sonogram, the quality of focusing was assessed, where:

A) For resolution test objects, which are the 120 μm hyperechoic strings positioned according to the scheme shown in Fig. 2. The RMS width of the angular intensity distribution was estimated using the formula:

$$\alpha = \sqrt{\frac{\int_a^b A(\varphi)(\varphi - \varphi_0)^2 d\varphi}{\int_a^b A(\varphi)d\varphi}} \tag{9}$$

where φ was the slope angle of the probing beam and φ_0 was the position of the peak intensity, and

$$\varphi_0 = \frac{\int_a^b A(\varphi)\varphi d\varphi}{\int_a^b A(\varphi)d\varphi} \tag{10}$$

where $A(\varphi)$ was the intensity distribution, while a and b were the integration limits determined by the intensity drop.

B) For the same objects, the peak intensity was calculated using the formula:

$$A_{\max} = \max\{A(\varphi)\} \tag{11}$$

For further analysis, see Table 1, which contains the correlation coefficients r for the aberration profiles obtained with the proposed method relative to those acquired with the reference method using the formula

$$r = \frac{\sum_{i=0}^{d-1} \Psi_{ref,i}\Psi_{prop,i}}{\sqrt{\sum_{i=0}^{d-1}\left|\Psi_{ref,i}\right|^2 \sum_{i=0}^{d-1}\left|\Psi_{prop,i}\right|^2}} \tag{12}$$

where i was the current number of the probe element, and Ψ_{ref} and Ψ_{prop} were the sets of correction delays obtained using the reference and proposed method, respectively.

In addition, to explore the relationship between the quality of correction and the number of lines and correction angles, the investigation was conducted using the medial target and aberrator #1 as an example. To achieve this, the number of lines varied from 1 to 40 while maintaining a fixed correction angle of 0.2°. Subsequently, the

Table 1 Correlation coefficient values for the phase distortion curves relative to the curves obtained using the reference correction method

Correction method	Type of target	Aberrator #1	Aberrator #2	Aberrator #3
Reference	Entire frame	1.000	1.000	1.000
Proposed	Close	0.854	0.709	0.446
	Medial	0.784	0.449	0.696
	Lateral	− 0.271	−0.738	0.755

correction angle was adjusted within the range of 1° to 2° while keeping the number of lines constant at 40.

Results

Figure 3 demonstrates fragments of the sonograms with the target objects before and after aberration correction. The right column in Fig. 3 displays all three targets in their undistorted states. The left column demonstrates the effect of defocusing, resulting in the doubling of targets caused by aberrator #1. The subsequent column exhibits the target tripling induced by aberrator #2. The column "Aberrator #3" shows signs of defocusing due to the passage of the wave through an *ex-vivo* bone. It is important to note that the presence of distortion layers significantly reduces the signal's dynamic range for all aberrators. In most cases, the angular width can be narrowed using either of the correction methods.

Figure 4 shows the instances of dependence of angular intensity distribution obtained from the same data as the fragments of sonograms in Fig. 3. In the presented instances for the medial target and aberrator #1, both correction methods gave approximately the same results. Notably, for most of the studied targets, the proposed method surpassed the reference one.

Based on the plots in Fig. 4, the numerical criteria for focusing quality were calculated and presented in Fig. 5. The value of parameter α increased while the value A_{max} decreased in the presence of aberrations. The largest

deviation of the mean value of the parameter A_{max} was recorded for the close target with aberrator #2 and amounted to 2.791 times for the proposed method relative to the case without correction. Meanwhile, the reference method for this target showed a slight decrease in A_{max} relative to the case without correction. The worst result was obtained for aberrator #2 and the lateral target when corrected by the reference method, where the mean value of A_{max} changed by 0.682 times; in contrast, when corrected by the proposed method, this target showed an improvement of 1.764 times compared to the case without correction. The experiments demonstrated the potential to reduce the RMS width of angular distribution by up to 58% when comparing the data without correction to the data obtained employing the proposed method for aberration correction for the close target and aberrator #1.

Figure 6 and 7 illustrate the sets of phase delays employed to adjust the focus and compensate for the aberration effect. The phase shifts in Fig. 6 were obtained using the proposed method, while the curves in Fig. 7 were obtained employing the reference aberration correction method. The phase delay sets from Fig. 6 were utilised to generate the sonograms shown in Fig. 3. It is evident from Fig. 6 that the sets of phase delays were unique and not repeated. Furthermore, for aberrator #1, the phase spread of two out of three targets did not exceed the range of -50° to 50°. For aberrator #3, the phase spread remained within the range of − 70° to 50°, and for aberrator #2, the phase spread of two out of three targets fell within the range of − 220° to 250°. It is worth noting that the reference

Type of target	Correction method	Aberrator #1	Aberrator #2	Aberrator #3	Without aberrator
Close	Without correction				
Close	Reference				
Close	Proposed				
Medial	Without correction				
Medial	Reference				
Medial	Proposed				
Lateral	Without correction				
Lateral	Reference				
Lateral	Proposed				

Fig. 3 Instances of the sonogram fragments. The width is plotted in rays along the horizontal direction and the depth is plotted in samples along the vertical direction
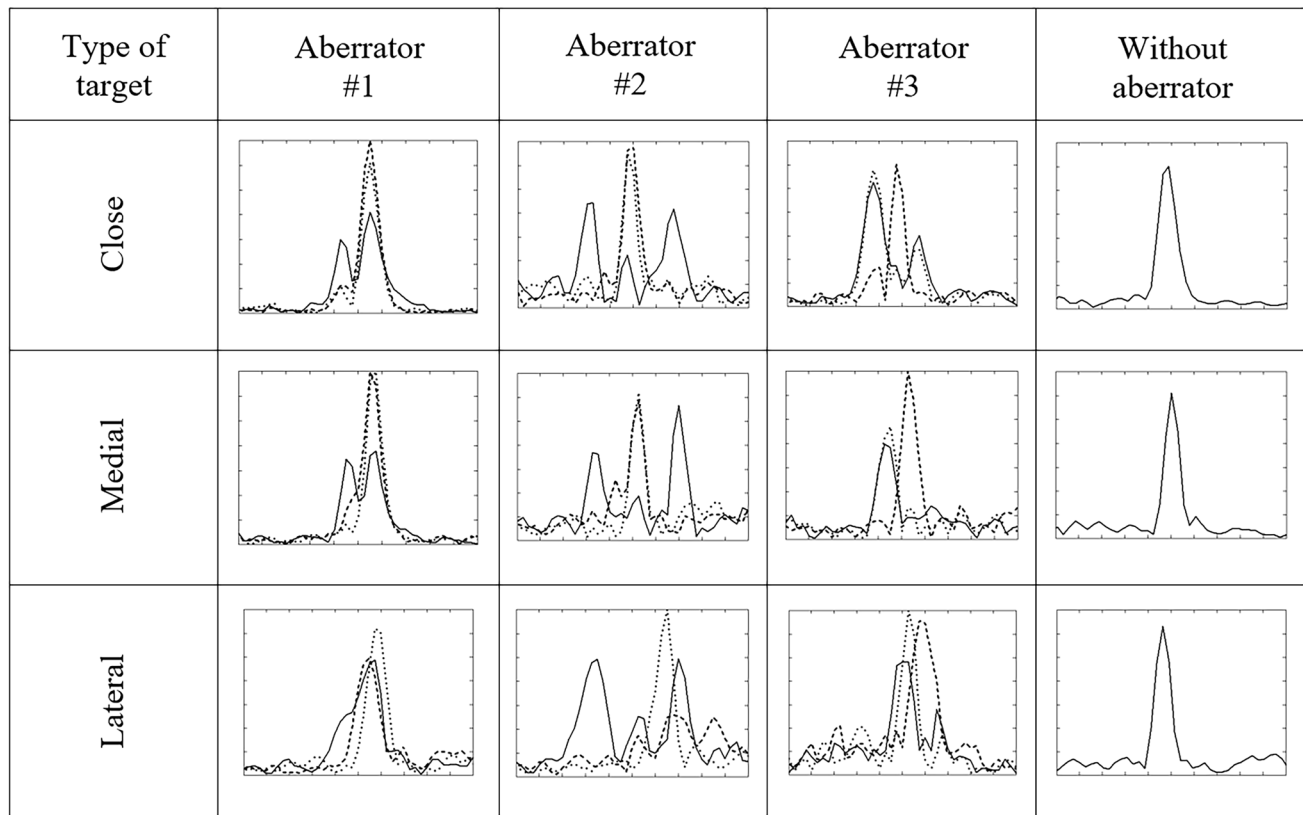
Type of target	Aberrator #1	Aberrator #2	Aberrator #3	Without aberrator
Close				
Medial				
Lateral				

Fig. 4 Dependence of the angular distribution of echo signal intensity with the 30° range for various scenarios: without correction (—); reference correction method (—); and proposed correction method (•••). The horizontal axis represents the angular coordinates ranging from − 15° to 15°, while the vertical axis represents the echo signal intensity. The curves correspond to the instances depicted in Fig. 3

method for aberration correction only allows for the calculation of a single set of delays for the entire frame.

Table 1 presents the correlation coefficient values between the sets of phase delays obtained using the proposed correction method and the curves generated by the reference correction method. The curve that closely matches the reference curve was obtained for the close target and aberrator #1, with a corresponding correlation coefficient of 0.854.

Figure 8 illustrates the relationship between the angular intensity distribution and the correction angle, as well as the number of lines utilised for correction. During the experiment, the greatest peak intensity was observed when employing the highest number of lines, which amounted to 40. This value exceeded the peak intensity achieved with 30 lines by 5.4%. Notably, the highest intensity was attained at a correction angle of 0.2°, and any deviation from this value led to a decrease in intensity.

Discussion

The paper investigated the possibility of applying a new method for the correction of ultrasound signal aberrations. The experiments were conducted using a scanner with a 64-element phased array probe operating in the synthetic aperture mode at a centre frequency of 2 MHz and an ATS phantom designed to test the resolution. By testing the method on targets positioned in different areas of the phantom (*i.e.,* close, medial, and lateral), it was demonstrated that phase distortions can be effectively corrected. To evaluate the outcomes, quantitative focusing quality criteria were employed to compare the results obtained using both the proposed and reference methods, as well as the uncorrected cases. This comparison revealed promising results.
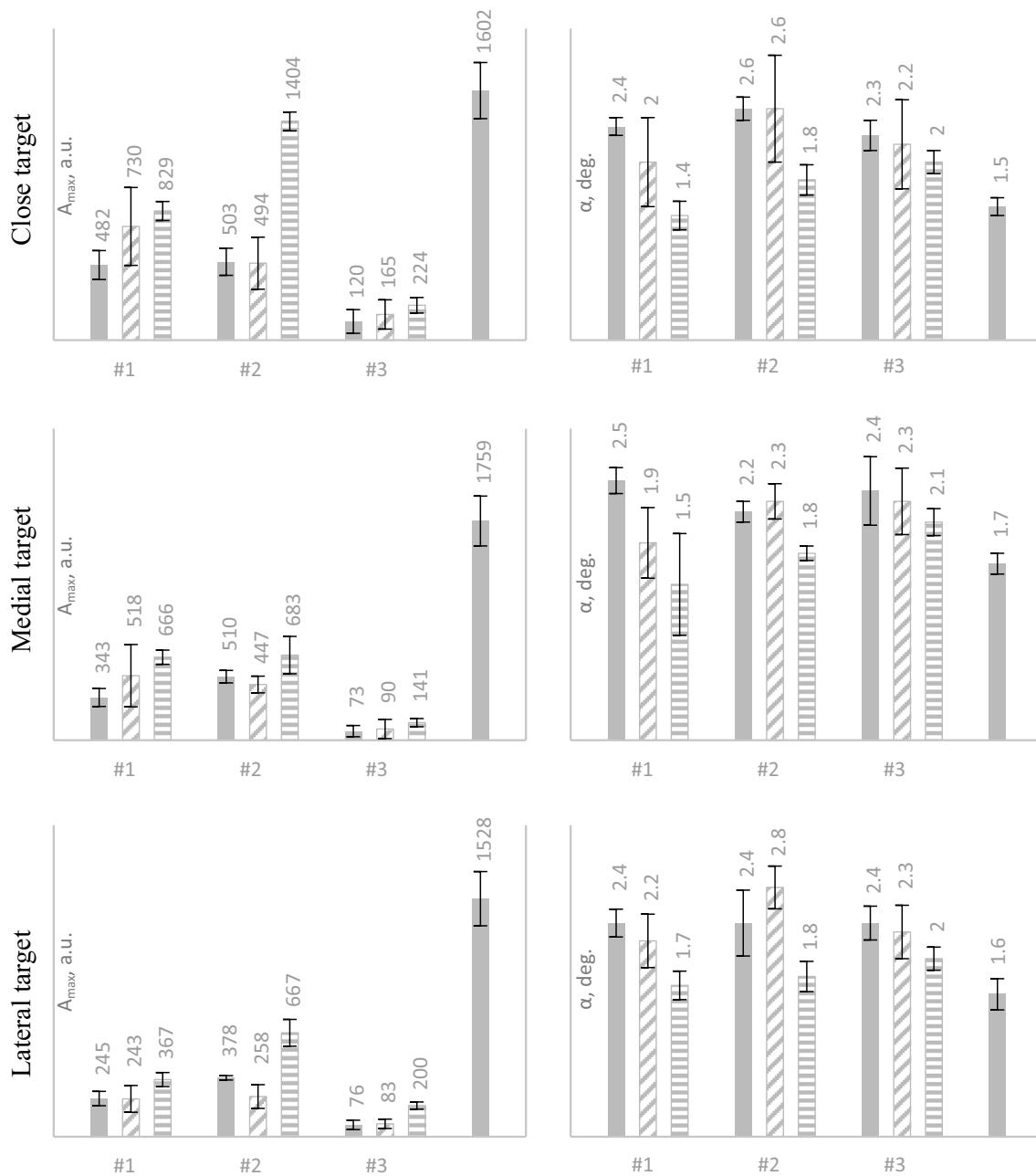
Fig. 5 Focusing quality criteria: RMS (α) and peak (A_{max}) angular intensity distribution of the echo signal for the case without any correction (■), as well as the cases corrected using the reference method (▨) and the proposed method (▤). These evaluations were conducted considering three distorting layers and the case where no aberrator was present

The peak intensity of the echo signal (A_{max}) and the width of the angular intensity distribution (α) were used to evaluate the performance of the algorithms. The rationale behind selecting these metrics is presented in the following paragraph.

The greater the peak intensity of the echo signal the more energy is restored through the aberration correction process. The width of the angular distribution decreases as the sidelobes diminish. Therefore, higher peak intensity and

narrower width of the angular distribution compared to the pre-correction case indicate that the aberration correction method has achieved a sharp focus.

Based on the information presented in Fig. 5, it was observed that, in certain cases, when an aberrator was present and the correction procedure was performed, the RMS width of the angular distribution α was smaller compared to when no aberrator was present. However, this does not necessarily imply that focusing after correction is superior
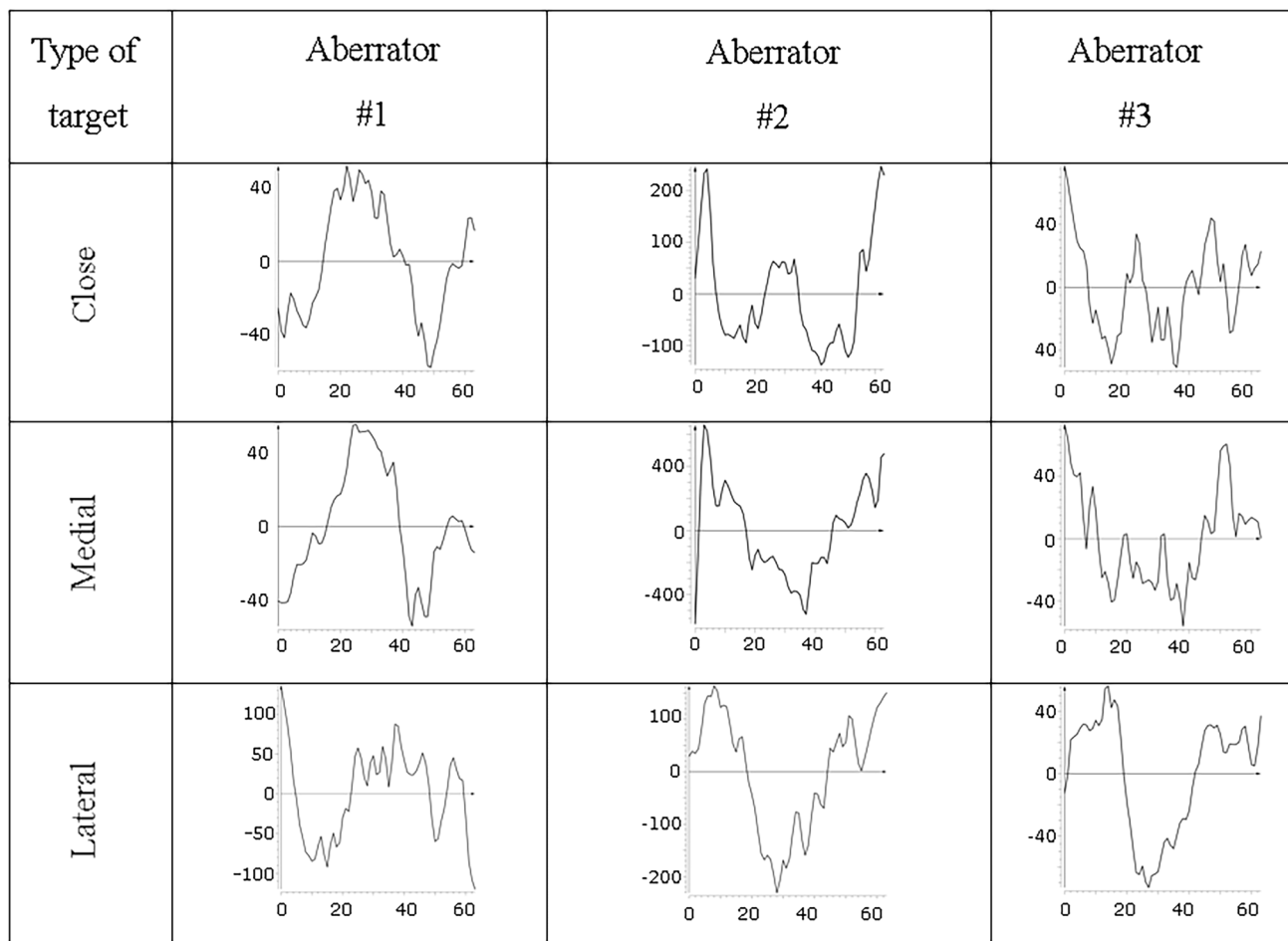
Fig. 6 Estimation of the dependence of phase distortions on the element number depending on the target and aberrator. The element number is plotted on the horizontal axis, and the phase shift in degrees is plotted on the vertical axis

to that without a distortion layer. This result is attributed to the energy loss that occurs when the ultrasonic wave passes through the distortion layer and at the interface, which causes a decrease in the peak intensity value A_{max} resulting in a reduction of the α value.
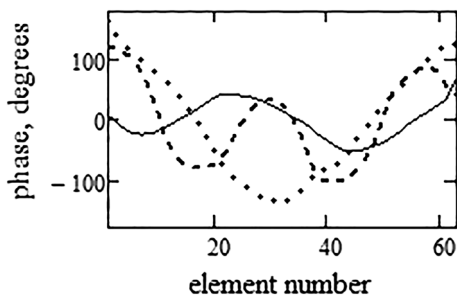
Fig. 7 Curves of the phase shifts estimated with the reference method for aberration correction with aberrator #1 (—), aberrator #2 (—), and aberrator #3 (•••)

The data presented in Table 1 demonstrate a weak correlation between the phase correction curves obtained using the proposed method and the reference method for phase aberration correction. The correlation coefficient was not close to 1.000, with the highest value being 0.854 obtained for the close target and aberrator #1. In this experiment, the RMS width of the angular distribution was 6.3% larger and the peak value was 12.9% lower compared to the reference correction value. Additionally, the lowest correlation coefficient was observed for phase corrections performed on the lateral target with aberrator #2. When comparing the performance of the proposed method with the reference method for this target, using the aberration presence criteria shown in Fig. 5. It was observed that the proposed method achieved a 25% improvement in the RMS width and a 1.764-fold increase in the peak value of the echo intensity distribution. In contrast, the reference method resulted in a degradation of both parameters when compared to the uncorrected data. For both targets, negative correlation coefficients were observed with aberrator #1 and #2. A negative correlation
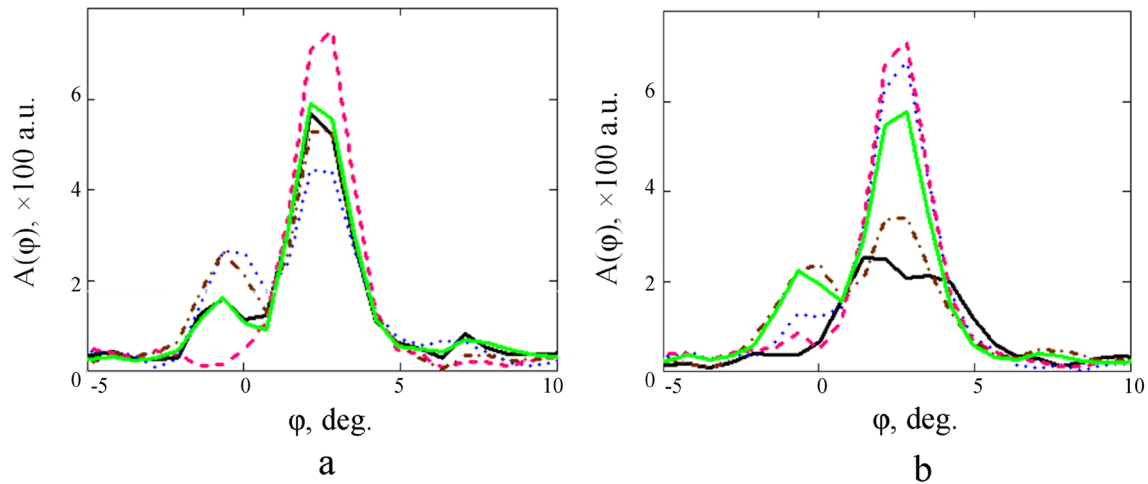
Fig. 8 Dependencies of the angular intensity distribution: **a** on the correction angle: $-1°$ (—), $-0.5°$ (•••), $0.2°$ (—), $1°$ (-•-), and $2°$ (—); **b** on the number of lines at the correction angle of $0.2°$: 1 (—); 4 (-•-); 15 (—); 30 (•••); and 40 (—)

indicates an inverse relationship, meaning that an increase in the curve generated by the proposed method corresponds to a decrease in the curve obtained with the reference method. In these cases, the results of the correction using the proposed method were more successful than with the reference method. This can be attributed to the lateral target's position away from the axis between the probes, which highlights the adaptability of the proposed method.

Figure 8 illustrates the curves representing the angular intensity distribution obtained for the medial target and aberrator #1. Upon analysing this figure, it becomes apparent that the peak value was influenced by both the angle and the number of correction lines.. Deviating from the optimal values of $0.2°$ and the maximum number of lines leads to the emergence of a side lobe on the left side of the target, thereby degrading the resolution.

The paper represents an advancement of research on the subject of aberration correction [9, 25], as it introduces a simple yet effective method to reduce phase distortions. It is necessary to employ high transmit pressures to compensate for the losses caused by the bone's high reflection and attenuation when using this approach for imaging through the skull. Therefore, this approach can be used for aberration estimation, involving the calculation of a distortion curve as depicted in Fig. 6. The resulting curve can be utilised to correct aberrations during a conventional firing event [22] when the complete set of array elements is used. However, if elements of the array are employed for transmission separately as it is usually done in the synthetic aperture method, they will not generate sufficiently high pressures, which will consequently result in a degradation of image quality.

The proposed method demonstrated a relatively fast processing speed. In our experiments, the time required to generate a sonogram in the synthetic aperture mode

without aberration correction averaged 8.580 ± 0.503 s. Comparatively, the reference correction method took 9.314 ± 0.530 s, while the proposed method took 9.051 ± 0.542 to generate a corrected image. However, a limitation of the method proposed in this study is that its implementation necessitates the use of an aperture synthesis mode and access to raw RF data, which restricts its applicability in conventional scanners.

In the future, the proposed method will undergo testing for the simultaneous correction of the entire frame. It is important to note that achieving high-quality correction for the entire frame requires each beam to have at least one unique set of correction delays. Additionally, the dependence of phase distortions on depth is not as explicit as it is on beam number [15, 16]. Moreover, the reference method and its variations, which are considered the "gold standard" in ultrasound imaging, necessitate the use of two coaxially located probes. This setup limits the applicability of the reference method as it cannot correct the entire frame in many imaging scenarios as correction would require repositioning the calibration probe. Therefore, the proposed method for aberration correction offers a broader range of applications compared to the reference method.

Directly comparing the results obtained in this study with those of other researchers [14, 15, 21, 25] was challenging due to the use of different metrics by various scientific groups and the fact that each group either collected its own dataset or employed a custom ultrasound machine for real-time testing. However, for those interested in reproducing the results obtained in this study or comparing the proposed method to other aberration correction methods, a publicly available ultrasound dataset can be utilised. Additionally, there is an option to either run C++ code in MS Visual Studio or use the executable file of our dedicated open-source

software, which implements aberration correction based on the proposed method [31].

Conclusion

The presented technique offers significant performance improvements and holds great potential for addressing critical clinical issues associated with ultrasound. Future research can focus on expanding the scope of correction and testing the method in *in-vivo* studies, as the wire targets used in the phantom were solely employed for demonstration purposes and are not crucial to the functionality of the proposed technique.

Declarations

Conflict of interest All authors declare no relevant conflict of interest.

Ethical approval This article does not contain any studies with human participants or animals performed by any of the authors.

References

1. Leonov D, Kulberg N, Yakovleva T, Solovyova P (2022) Approach to detecting aberrations in transcranial ultrasound imaging. Acoust Phys 68:175–186. https://doi.org/10.1134/S106377102202004X

2. Deng L, Hughes A, Hynynen K (2020) A noninvasive ultrasound resonance method for detecting skull induced phase shifts may provide a signal for adaptive focusing. IEEE Trans Biomed Eng 67(9):2628–2637. https://doi.org/10.1109/TBME.2020.2967033

3. Aarnio J, Clement GT, Hynynen K (2005) A new ultrasound method for determining the acoustic phase shifts caused by the skull bone. Ultrasound Med Biol 31(6):771–780. https://doi.org/10.1016/j.ultrasmedbio.2005.01.019

4. White PJ, Clement GT, Hynynen K (2006) Local frequency dependence in transcranial ultrasound transmission. Phys Med Biol 51(9):2293–305. https://doi.org/10.1088/0031-9155/51/9/013

5. Ammi AY et al (2008) Characterization of ultrasound propagation through ex-vivo human temporal bone. UMB 34(10):1578–1589. https://doi.org/10.1016/j.ultrasmedbio.2008.02.012

6. O'Donnell M, Flax SW (1988) Phase-aberration correction using signals from point reflectors and diffuse scatterers: measurements. IEEE Trans Ultrason Ferroelectr Freq Control 35(6):768–774. https://doi.org/10.1109/58.9334

7. Nock L, Trahey GE, Smith SW (1989) Phase aberration correction in medical ultrasound using speckle brightness as a quality factor. J Acoust Soc Am 85(5):1819–1833. https://doi.org/10.1121/1.397889

8. Fink M et al (2000) Time-reversed acoustics. Rep Prog Phys 63(12):1933–1995. https://doi.org/10.1088/0034-4885/63/12/202

9. Kyriakou A, Neufeld E, Werner B, Paulides MM, Szekely G, Kuster N (2014) A review of numerical and experimental compensation techniques for skull-induced phase aberrations. Int J Hyperthermia 30(1):36–46. https://doi.org/10.3109/02656736.2013.861519

10. Clement GT, Hynynen K (2002) Correlation of ultrasound phase with physical skull properties. Ultrasound Med Biol 28(5):617–624. https://doi.org/10.1016/s0301-5629(02)00503-3

11. Tanter M, Aubry JF, Gerber J, Thomas JL, Fink M (2001) Optimal focusing by spatio-temporal inverse filter. I. Basic principles. J Acoust Soc Am 110(1):37–47. https://doi.org/10.1121/1.1377051

12. Pernot M, Montaldo G, Tanter M, Fink M (2006) 'Ultrasonic stars' for time-reversal focusing using induced cavitation bubbles. Appl Phys Lett 88(3):034102. https://doi.org/10.1063/1.2162700

13. Phillips DJ, Smith SW, von Ramm OT, Thurstone FL (1975) Sampled aperture techniques applied to B-mode echoencephalography. Acoust Hologr 6:103–120. https://doi.org/10.1007/978-1-4615-8216-8_6

14. Vignon F, Aubry JF, Tanter M, Margoum A, Fink M (2006) Adaptive focusing for transcranial ultrasound imaging using dual arrays. J Acoust Soc Am 120(5):2737–2745. https://doi.org/10.1121/1.2354073

15. Lindsey BD, Smith SW (2013) Pitch-catch phase aberration correction of multiple isoplanatic patches for 3-D transcranial ultrasound imaging. IEEE T-UFFC 60(3):463–480. https://doi.org/10.1109/TUFFC.2013.2590

16. Osipov LV et al (2021) Transcranial beam steering with aberration correction. Biomed Eng 54(6):438–442. https://doi.org/10.1007/s10527-021-10057-3

17. Kim J, Kasoji S, Durham PG, Dayton PA (2021) Acoustic holograms for directing arbitrary cavitation patterns. Appl Phys Lett 118:051902. https://doi.org/10.1063/5.0035298

18. Brown MD, Cox BT, Treeby BE (2020) Stackable acoustic holograms. Appl Phys Lett 116:261901. https://doi.org/10.1063/5.0009829

19. Aubry JF, Tanter M, Pernot M, Thomas JL, Fink M (2003) Experimental demonstration of noninvasive transskull adaptive focusing based on prior computed tomography scans. J Acoust Soc Am 113(1):84–93. https://doi.org/10.1121/1.1529663

20. Leung SA, Moore D, Gilbo Y, Snell J, Webb TD, Meyer CH, Miller GW, Ghanouni P, Butts Pauly K (2022) Comparison between MR and CT imaging used to correct for skull-induced phase aberrations during transcranial focused ultrasound. Sci Rep 12(1):13407. https://doi.org/10.1038/s41598-022-17319-4

21. Lambert W, Cobus LA, Frappart T, Fink M, Aubry A (2020) Distortion matrix approach for ultrasound imaging of random scattering media. Proc Nat Acad Sci USA 117(26):14645–14656. https://doi.org/10.1073/pnas.1921533117

22. Jensen JA, Nikolov SI, Gammelmark KL, Pedersen MH (2006) Synthetic aperture ultrasound imaging. Ultrasonics 44(Suppl 1):e5-15. https://doi.org/10.1016/j.ultras.2006.07.017

23. Passmann C, Ermert H (1996) A 100-MHz ultrasound imaging system for dermatologic and ophthalmologic diagnostics. IEEE T-UFFC 43(4):545–552. https://doi.org/10.1109/58.503714

24. Kulberg N, Leonov D (2021) Method for obtaining ultrasonic brain images. Patent RU 2750965

25. Tillett J, Astheimer J, Waag R (2010) A model of distributed phase aberration for deblurring phase estimated from scattering. IEEE T-UFFC 57:214–228. https://doi.org/10.1109/TUFFC.2010.1400

26. Benenson Z, Kulberg N, Elizarov A (1999) Algorithmic method for generation of a nondiffraction beam for constructing 3d high-resolution images in ultrasonic medical diagnostics. Pattern Recognit Image Analysis 9(3):492–504

27. Goodman JW (1968) Introduction to fourier optics. McGraw-Hill, New York

28. Leonov D, Kodenko M, Leichenco D, Nasibullina A, Kulberg N (2022) Design and validation of a phantom for transcranial ultrasonography. Int J Comput Assist Radiol Surg 17(9):1579–1588. https://doi.org/10.1007/s11548-022-02614-2

29. Fry FJ, Barger JE (1978) Acoustical properties of the human skull. J Acoust Soc Am 63(5):1576–1590. https://doi.org/10.1121/1.381852

30. Vignon F, Shi WT, Burcher MR, Powers JE (2008) Determination of temporal bone isoplanatic patch sizes for transcranial phase aberration correction. IEEE Ultrasonics Symp. https://doi.org/10.1109/ULTSYM.2008.0311

31. Aberration Correction: Raw Ultrasound Data and Computer Program. https://doi.org/10.6084/m9.figshare.18495170.v1